CHAPTER 5

Cosmic Ray Test

Since the SuperKEKB accelerator upgrade was not yet finish, the cosmic ray detection was used to test the inner chamber with the readout electronic prototype [7]. The detector setup and the detection result are described in this chapter.

5.1 Detector Setup

First of all, the gas was set to 50% He/ 50%C_2H_6 at the relative pressure of 5.8 mmH_2O per 1 atm room pressure with the gas flow rate of 30 cc/min and 47 % humidity. Even through, for in-beam operation, the gas controller system will be keep at an absolute pressure at 1 atm. To test the chamber, either the gas leak rate check or the cosmic ray test, the gas pressure is measured as the time dependence of the relative pressure between the atmosphere and the pressure in the chamber.

On the front end, the sense wire pins of each layer were connected by the cable to the power supply. A high voltage of 2.1 kV was supplied to the sense wires by carefully increase the voltage. The field wire pins are directly inserted to the endplates as the grounded level. To avoid the discharge on the outside of the chamber due to a very tiny distance between the sense wire pins and the end plate, plastic insulator tubes were covered all the sense wire pins for both front end and back end, and also, the high voltage connector.

After the chamber was connected with the high voltage for one day, the chamber can handle a stable voltage without any discharges. The leak current is approximately 80 nA or around 0.06 nA per wire. Then, the cabling for detecting the particle signals were connected on the back end. It can be described in two sections including the setup for trigger signal and the setup for the cosmic ray data collecting.The overview of the detector set up is shown in Figure 5.1.

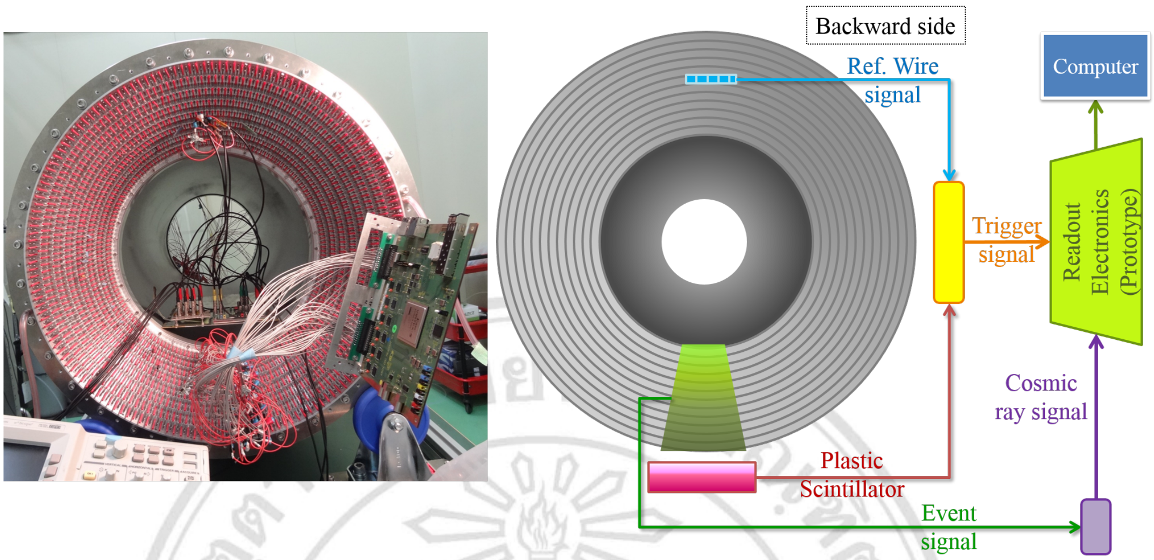

Figure 5.1: The overview of the detector setup for the cosmic ray detection.

5.1.1 Setup for trigger signal

In this experiment, only the charged particles from the cosmic ray, which passed through the central axis of the chamber in vertical direction were measured. A plastic scintillator counter and the reference wire layer were set for trigger signal generating. Figure 5.2 indicates a diagram of the chamber setup for the trigger signal generating.

The reference wires consist of 4 drift cells, which were arranged on the upper part of the chamber in the fourth layer. They were arranged on the vertical line passing the middle of the detector and on the same line as the plastic scintillator, which was located under the chamber (Figure 5.1). When a particle pass through the reference layer, the signal of the particle from the reference wire was shaping and amplifying by 1-chip ASIC board. The ASIC board sent the output positive signal with the square shape. Because the read out electronics requires the negative signal, the converter, which took a role to change the signal to be negative, was used. After that, the four cables of each reference wire were connected to the module, which merge all signals to be one. Then, the gate generator module was used to expand the signal width to 10 μs before it was transferred to the coincident module.

The particle passed through the chamber and hit the plastic scintillator counter. The signal from the counter was transferred to the discriminator module to be amplified and shaped to a negative square shape signal. The signal was delayed for 200 ns in order to force the signal to arrive the coincident module at almost the same time as the signal from the reference wires. This coincident signal from the reference wires and the scintillator counter was a trigger signal for the readout electronic. The analog signals from the reference wire, the scintillator counter and their coincident signal monitored by the oscilloscope are shown in Figure 5.2. To selected the signal from the chamber, the trigger signal has to be adjusted with an additional time delay from the chamber signal around 600 ns. The reason of this delay is described in section 5.1.2 .

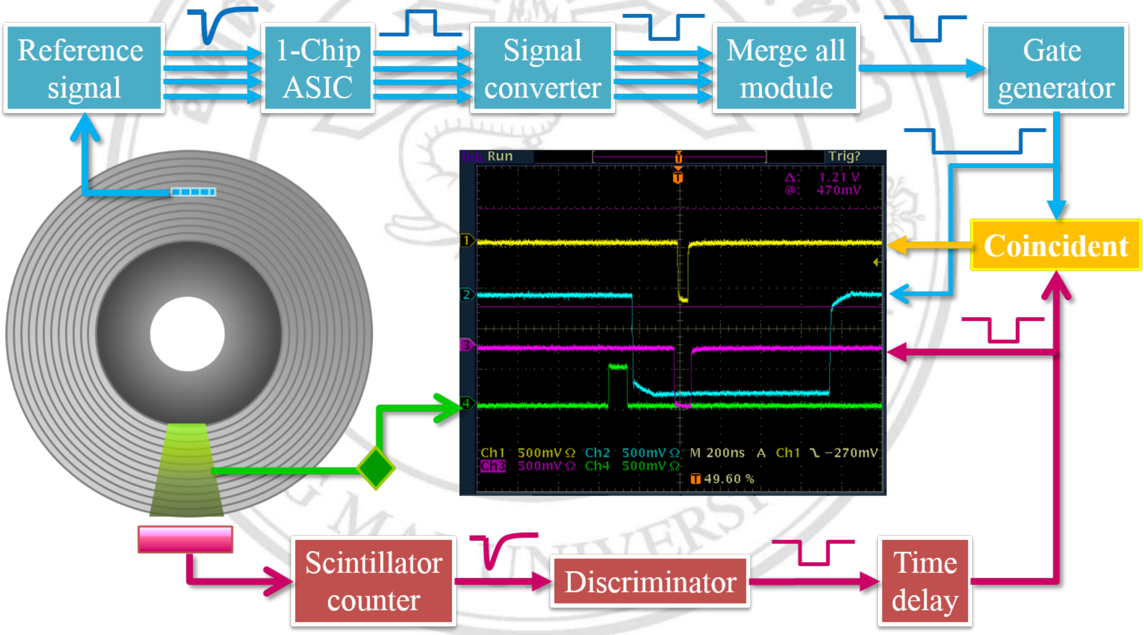

Figure 5.2: The diagram of the detector setup for trigger signal generating. The blue arrows represent the reference wire signal. the red arrows stand for the signal from the scintillator counter. An example amplified and shaped chamber signal from the 48 considered wires in the chamber, in the green area, is represented by the green arrow.

5.1.2 Setup for the cosmic ray data collecting

A readout electronic prototype board has 48 input channels. Therefore, six drift cells from each layer, which shared their positions near the same vertical path as the reference signal and the scintillator counter (the green area in figure 5.2), were chosen as the considered wire and connected to the readout electronics board. The chosen 48 drift cells were labeled as the channel numbers 0 to 47 from left to right and from the first layer, the innermost layer, to the eighth, outermost layer. The readout electronics has a main role to digitize the event signal and its timing to the data acquisition system (DAQ).

The signal from the chamber is digitized by a 32 MHz flash ADC (FADC) to collect an analog signal wavefrom. The size of this signal is corresponding to the charge caused by the ionization in the cell or the energy loss dE/dx, which the detail was described in Chapter 2. In this experiment, the time interval for collecting a signal, called the "time window", was set to 544 ns, including 17 data sampling with 32 ns step time for each series. Each data series contains the pulse height of each channel as shown in each row of the raw data format in section 5.2.1.

Time digital converter on the board includes the discriminator, which is used to digitize the time of the chamber signal with 1 ns resolution [2]. The data acquisition has to be triggered by the appropriate condition, which is determined by the whole Belle II detector in actual situation. Generally the trigger signal was delayed and the CDC has to keep the data during the decision. The trigger delay Figure 5.3 is adjustable in the range from 0μ m to 8 μm [7]. It was set to be 544 ns for this experiment, which was related to the delay setting in section 5.1.1. The timing data was measure between the time that the sense wire can detect the incoming particle signal, called "hit time", and the trigger time. The time interval between the hit time and the trigger time is called "TDC time". The TDC time was used in drift time calculation. Figure 5.3 presents the time measurement procedure and the collected signal wavefrom.

After the signal was triggered and the chamber signal sent to the readout board, both signal information and timing were digitized to the FADC variable data and the TDC time data, respectively. The data was transferred through an optical fiber to the hub, which transfer the data through a LAN cable to a computer. In addition, the chamber was covered by a copper net as a Faraday cage to avoid the electromagnetic noise. All data collections took various duration depending on number of events and the probability of the incoming cosmic ray.

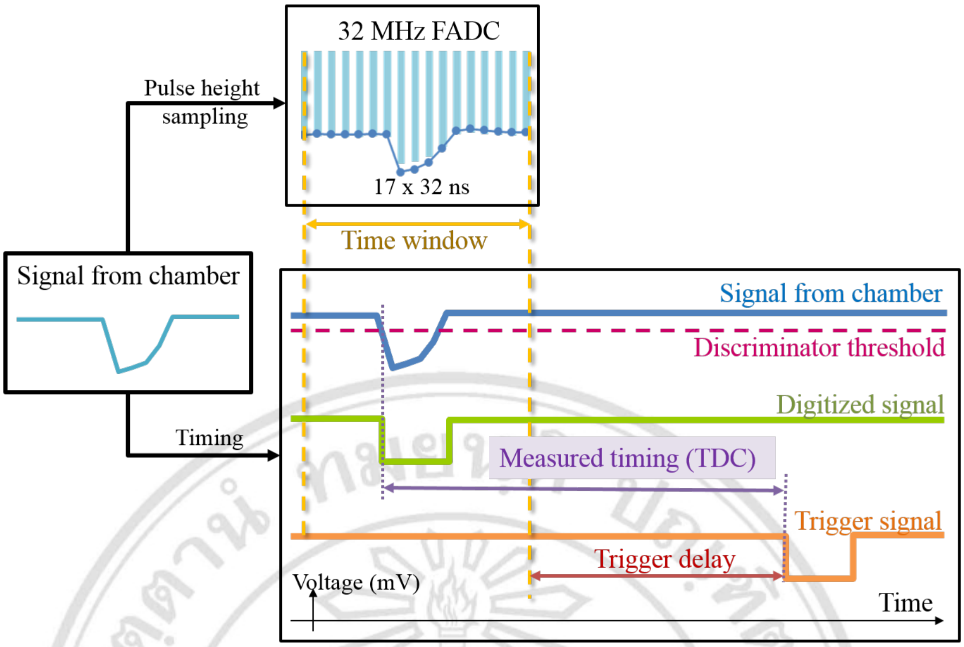

Figure 5.3: The diagram of the time measurement procedure and the collected signal waveform

5.2 Raw Data Interpretation

In this section, raw data format were presented. The analysis of the chamber signal pulse high related to the generated charge as well as the calculation of the drift time from the TDC time were also described.

5.2.1 Data Format

The data was save as $.DAT$ file format. An example of the data is shown in the figure 5.4. In each event, it begins with the header, which includes the name of event, called *Trigger#...(run number)..* . The data consists of 96 columns divided to 48 columns, from 0 to 47 related to the labeled drift cell (channel), for the FADC data and the others for timing data. For this experiment, the FADC data consists of 17 rows as time window setting. The timing data starts first row with the trigger time, then, the fastest hit time (T_1) and the second-fastest hit time (T_2), if it has. All variables are written in hexadecimal number.

The interpretation of the raw data started by data conversion from hexadecimal number to decimal number and then its format was charged to more simple arrangement. All calculation and plot were done by using the ROOT program and all program were written in C++.

5.2.2 Generation of Charged Distribution

The FADC variable contains information of the signal pulse by collecting the amplitude of the signal in each step time. In this study the step time was set as 32 ns. However, the FADC variables also include the electric noise and fluctuation with the condition of the shaper of the readout electronics, which is called the pedestal. As mentioned earlier that the pedestal was collected before applying the high voltage for the cosmic ray data collecting. Too many number of events collecting can cause the error from the variation of the pedestal in time. Hence, in this experiment, the number of events were set in order of thousand, which took about one day to collect the data. For this analysis, totally 37,491 events from eight times collection, were taken in to account. Since the electronic noise was slightly fluctuate in time, thus, the background was collected every time prior the cosmic ray data collection. For actual in-beam experiment, the pedestal data is taken day by day. Figure 5.5 indicates the diagram of the generated charge analysis procedure. As shown in the figure, the pedestal (yellow area) shifts the signal pulse from zero. The charge, which is produced by the ionization in the cell, was calculated by subtracting the mean value of the pedestal from the raw FADC data. Then, the selection non-zero data process was performed by adding a threshold data. The next step was the summation of the selected data. The summation were filled in the distribution plot of its channel. The variable of FADC summation is corresponding to the generated charge analysis and also to the energy loss dE/dx. Thus, the distribution was generated with the landau shape (see section 2.2). The peak corresponds to the most probable energy loss.

The distribution plot of FADC summation was required in order to verify that the readout electronic board and the inner chamber were working well for the generated charge analysi. Due to the difference in shape of each drift cell layer and probable fluctuation of electronic condition of the board, the FADC summation distribution have to be checked

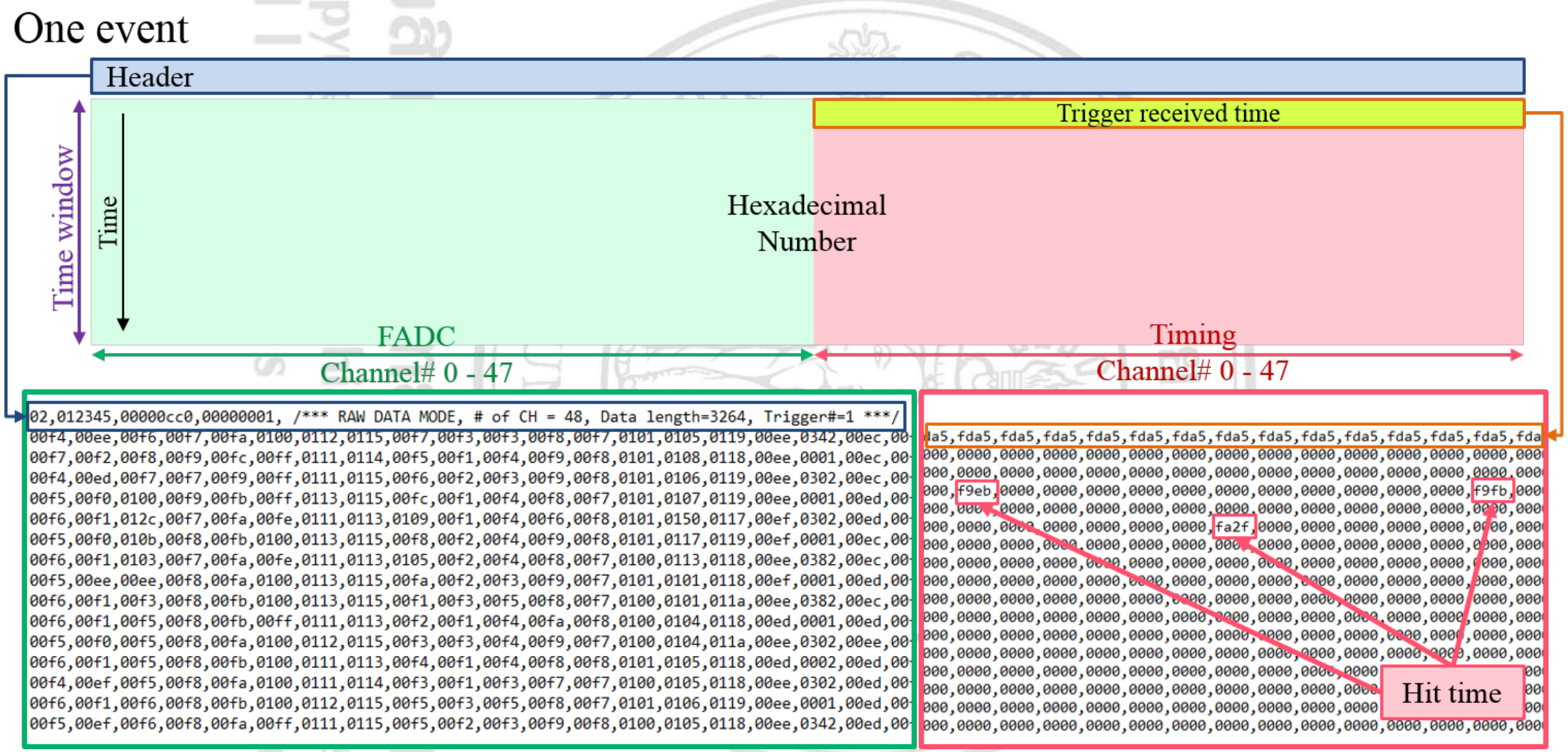

Figure 5.4: Overview of the raw data format.

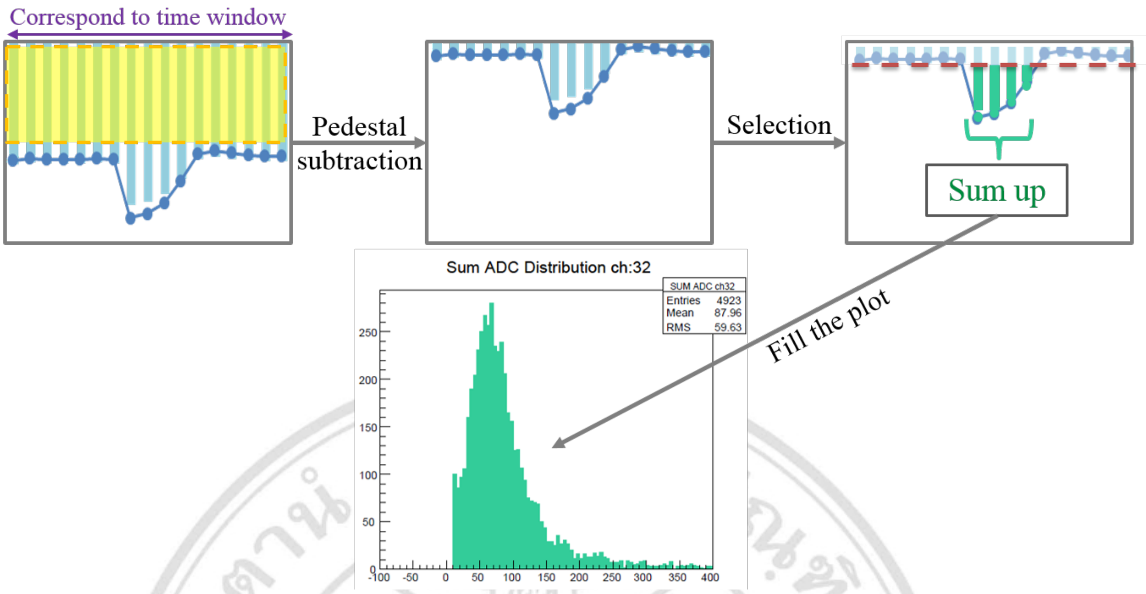

Figure 5.5: The diagram of the procedure of the generated charge analysis

channel by channel. Figure 5.6 - 5.13 show the summation of the FADC distribution from each channel of the inner chamber.

Although, the overview of the distribution for all layer has the landua shape, the innermost layer and the outermost layer distributions are large. This is because the drift cells are close to the inner cylinder and the temporary outer aluminum cylinder cover which is covered with the ground potential, which the electric field of both layers are distorted. Since the pedestal subtraction and the threshold selection are insufficient, some small peaks at the front edge of the landau distribution from the pedestal still occurred. The distribution channel 17 and 22 are invalid in the considered region. In contrast, these problems are disappeared in the timing data. The analyzed timing results will be described in section 5.2.3. Therefore, these problems were probably caused by the amplification gain in the readout electronics or the non-proper adjustment of the time window and the trigger time delay.

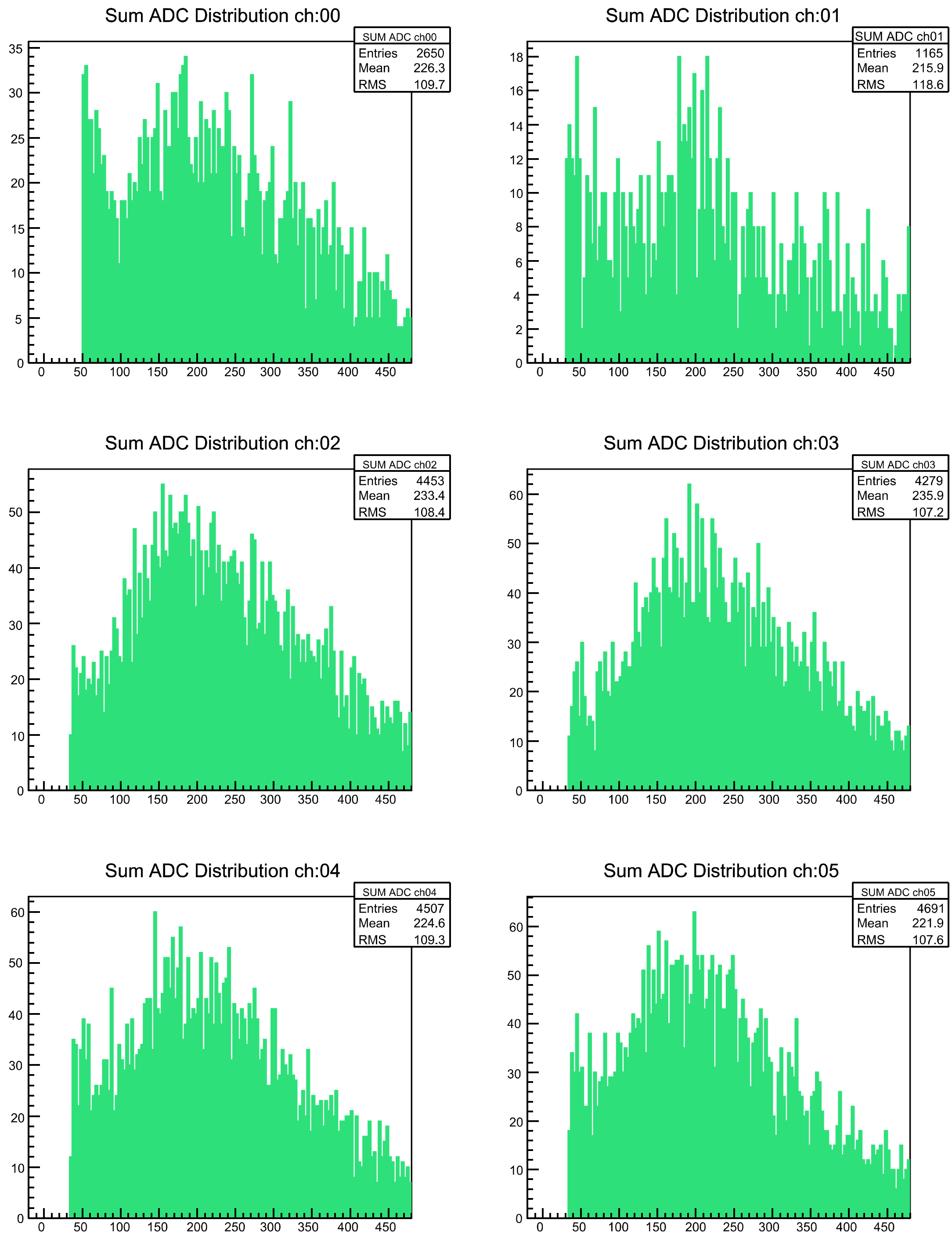

Figure 5.6: The FADC summation distribution (ch. 0 - 5).

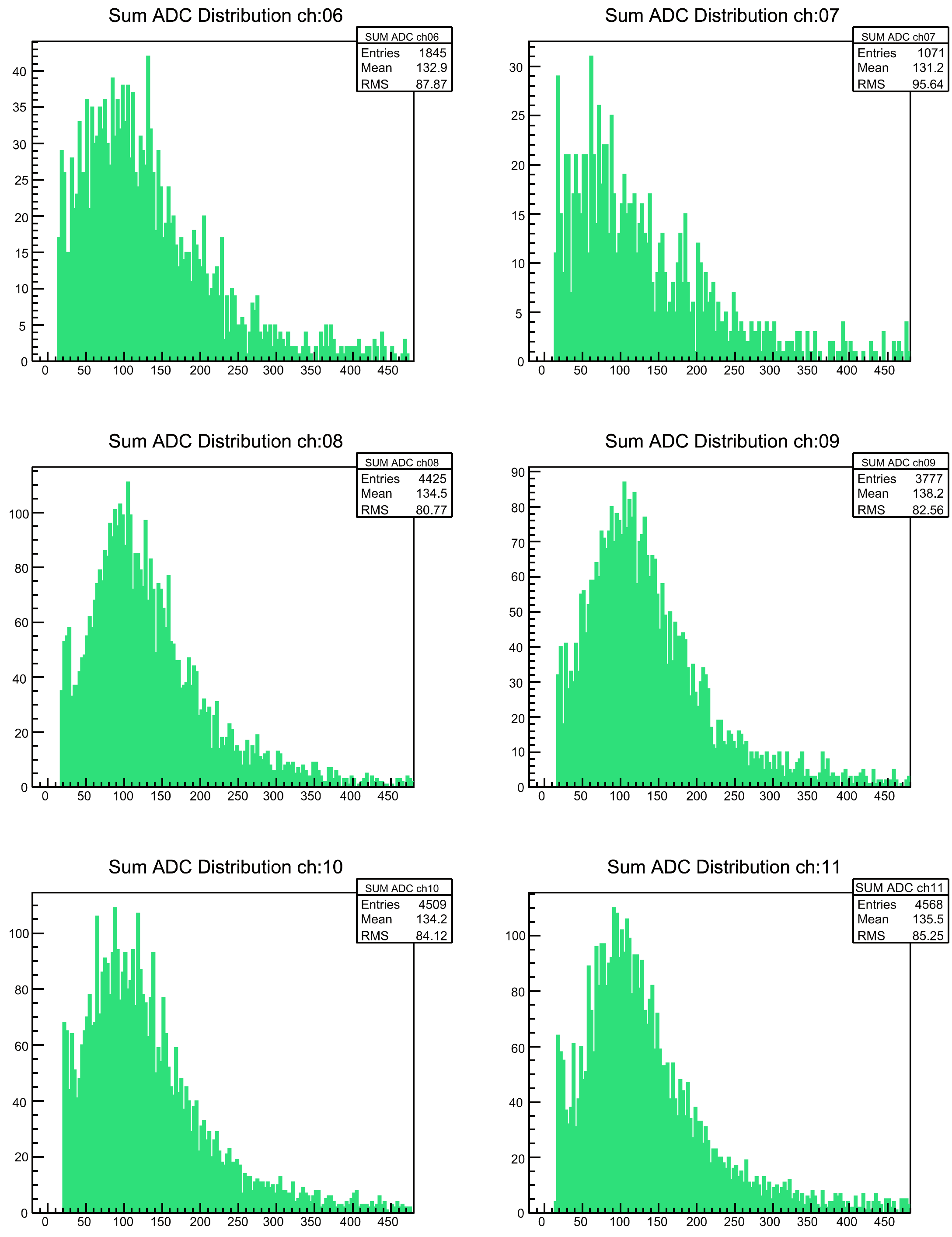

Figure 5.7: The FADC summation distribution (ch. 6 - 11).

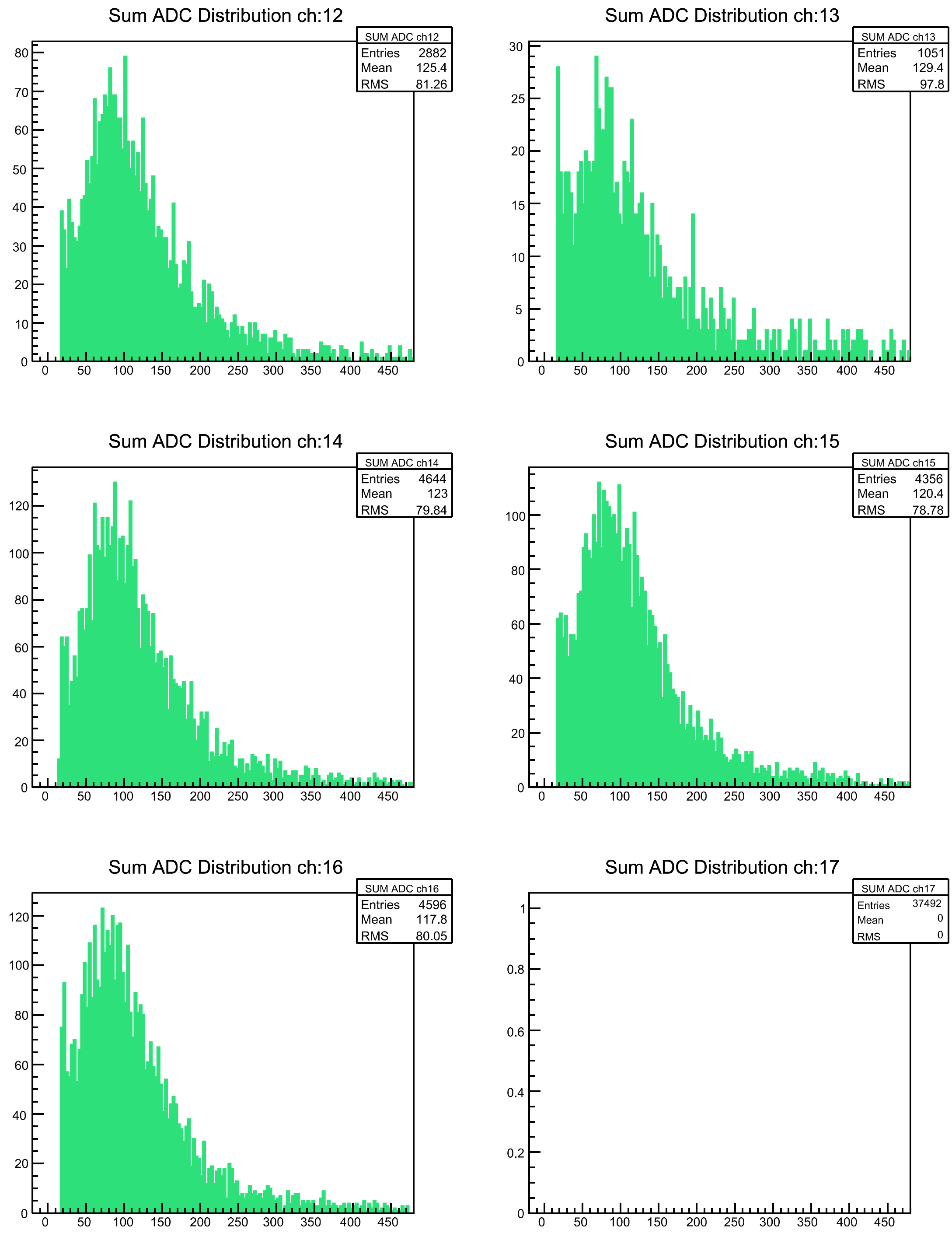

Figure 5.8: The FADC summation distribution (ch. 12 - 17).

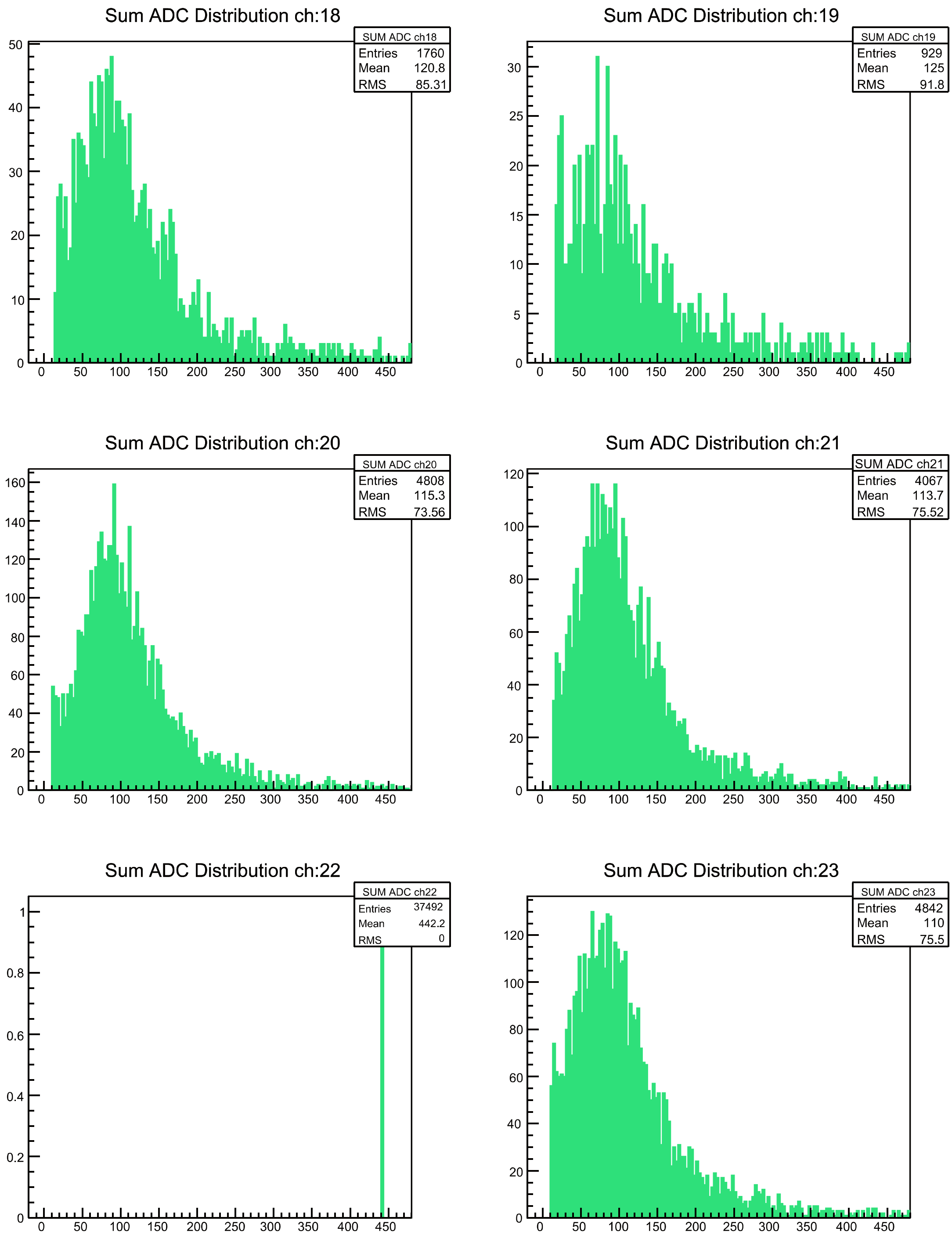

Figure 5.9: The FADC summation distribution (ch. 18 - 23).

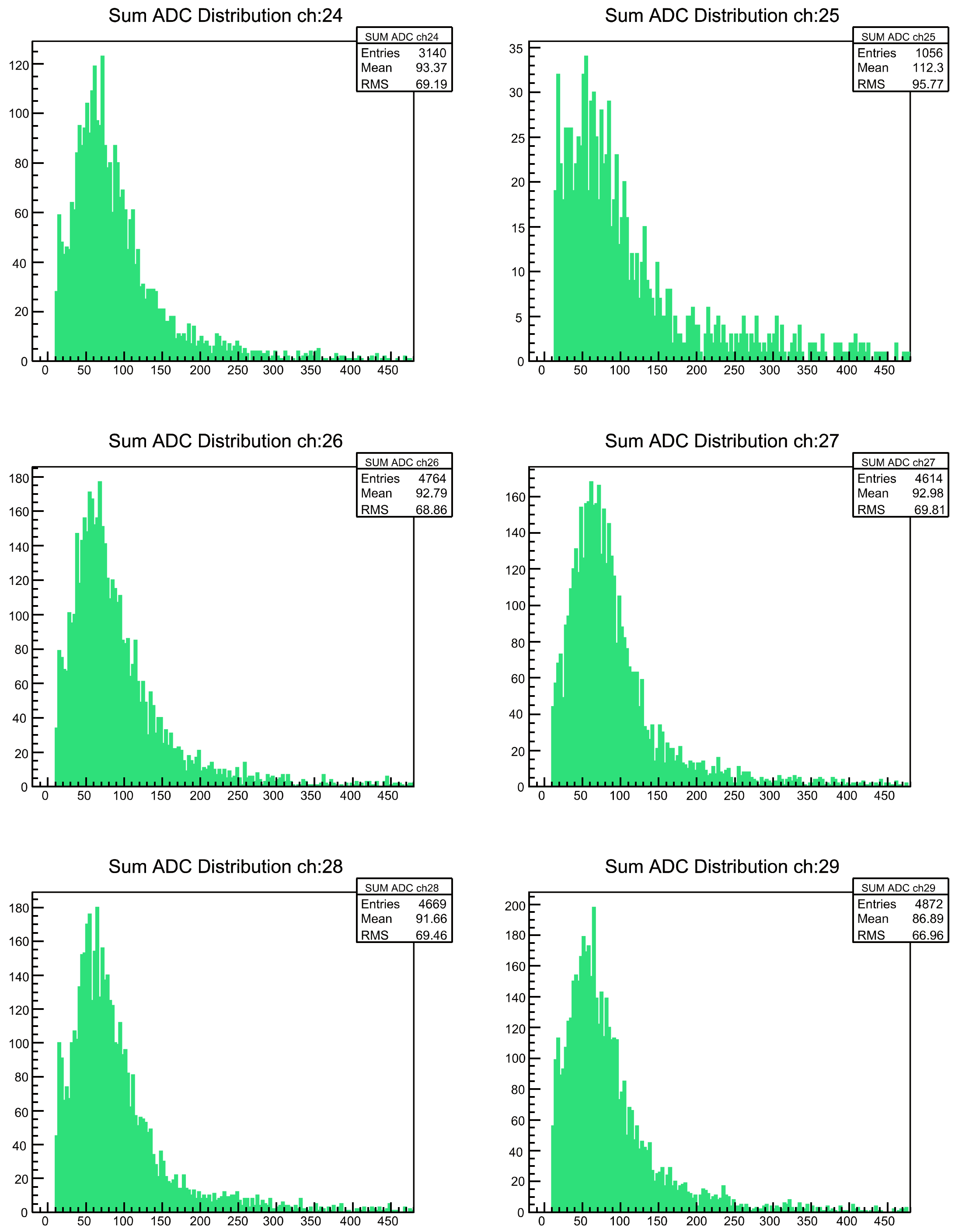

Figure 5.10: The FADC summation distribution (ch. 24 - 29).

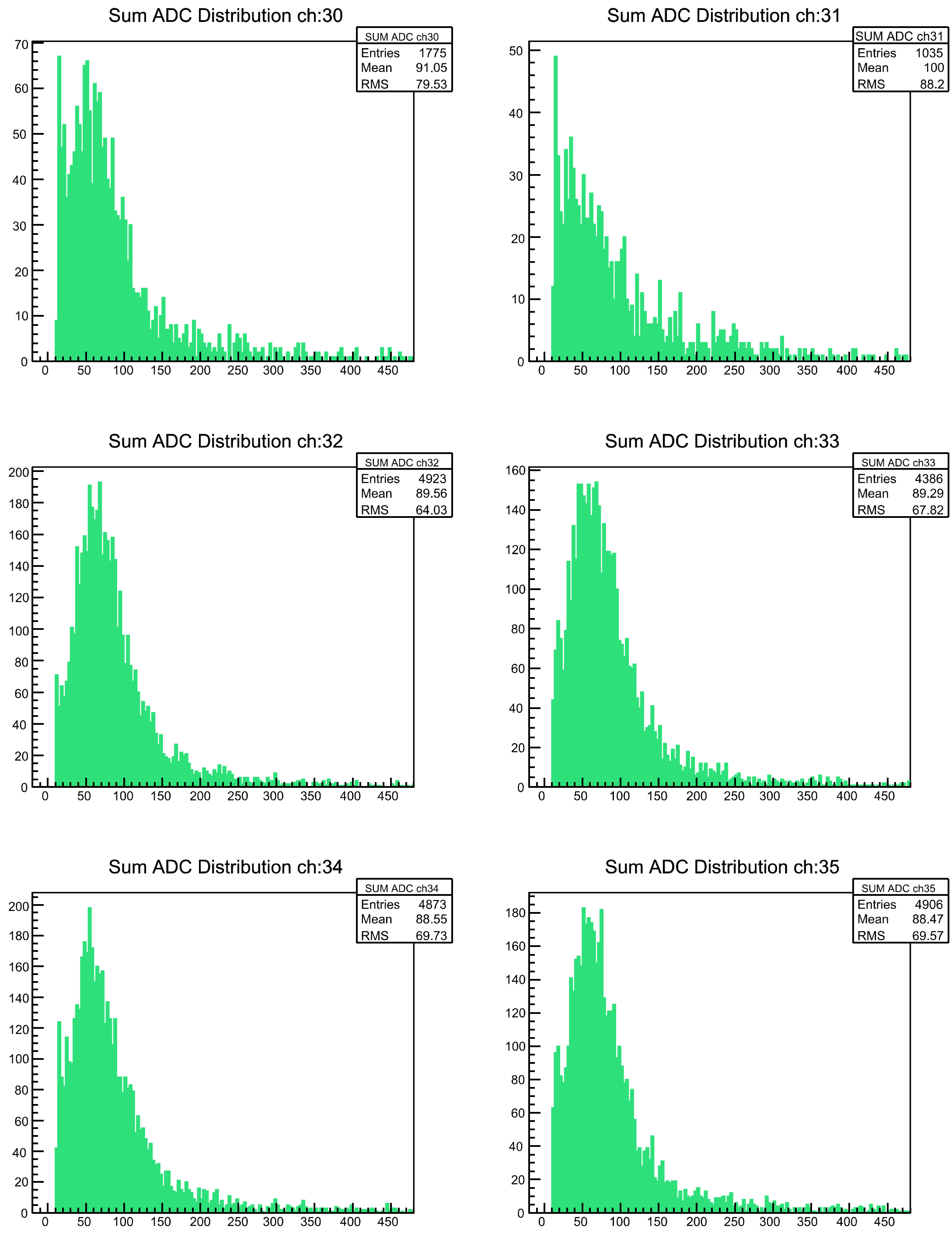

Figure 5.11: The FADC summation distribution (ch. 30 - 36).

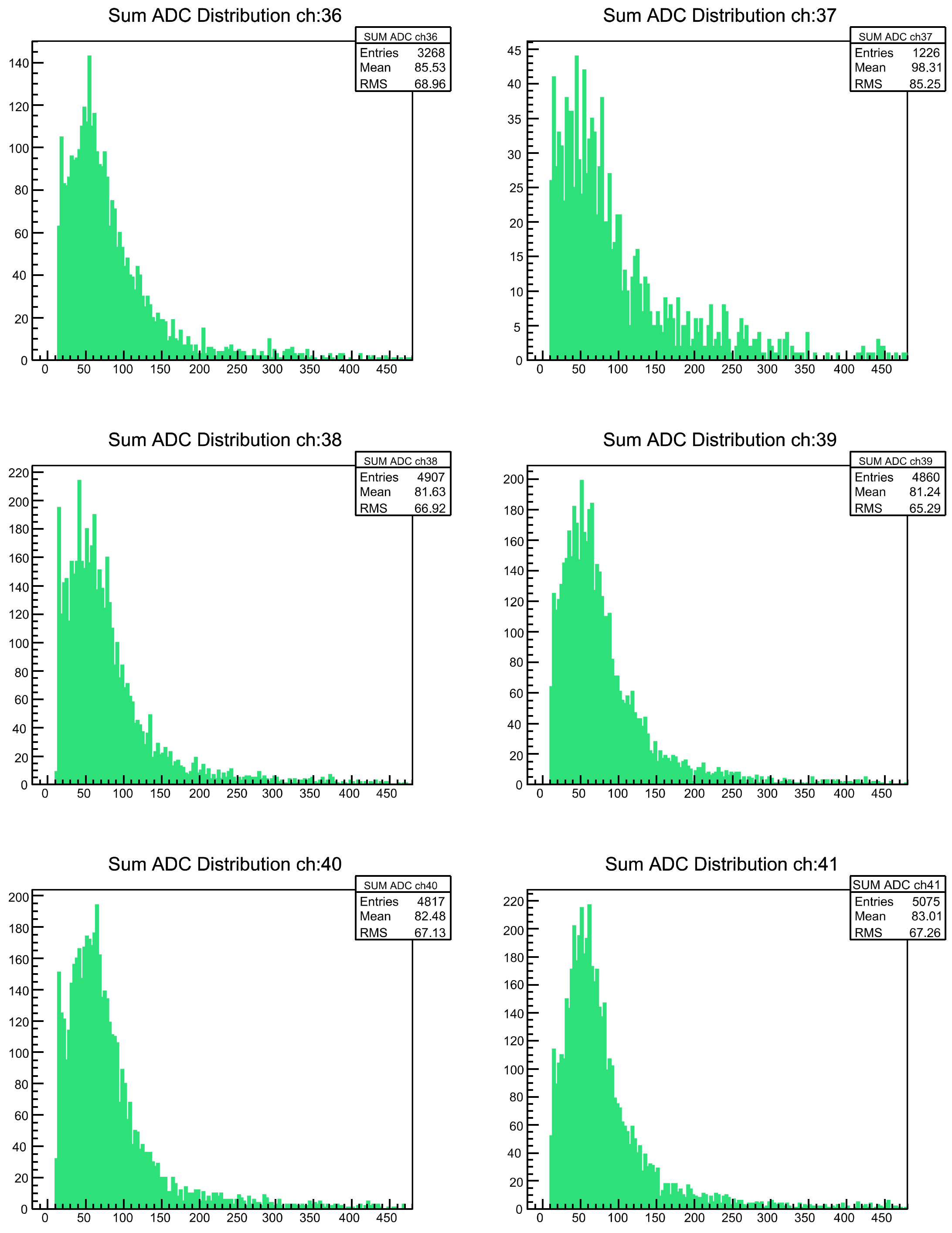

Figure 5.12: The FADC summation distribution (ch. 37 - 42).

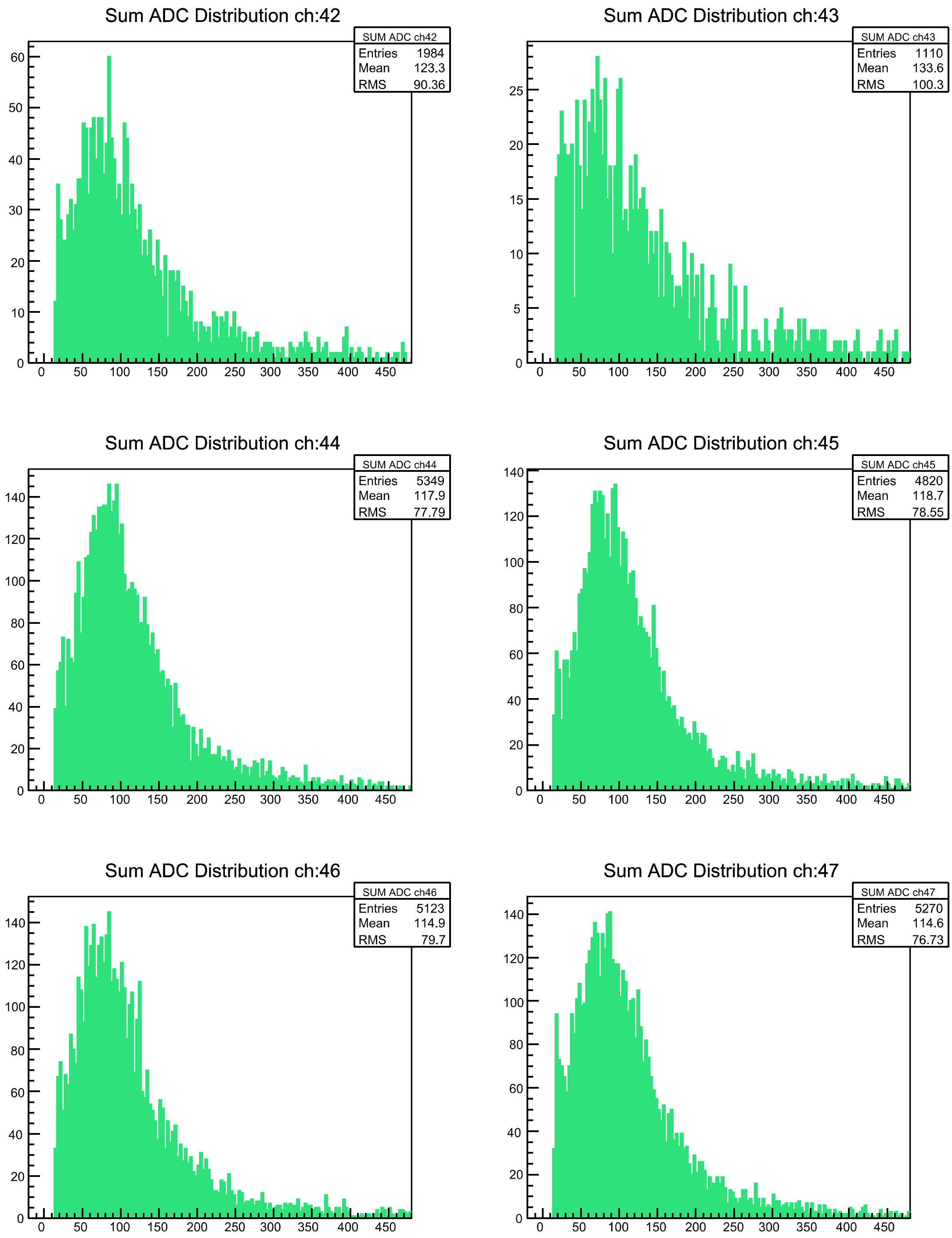

Figure 5.13: The FADC summation distribution (Ch. 43 - 47).

5.2.3 Drift Time Measurement

In order to analyze the timing data, the event data were filtered out from the electronics noise and some incomplete data. According to the trigger time setting, the hit time, which comes faster than the delayed trigger time (less than 750 ns) was cut off. This experiment considered only the event that provided only one fastest hit time ($T1$) to study the drift time. Figure 5.14 presents the distribution of the hit times in one channel. There is about 79% of the drift cells, which provide the one hit time, and the others were neglected.

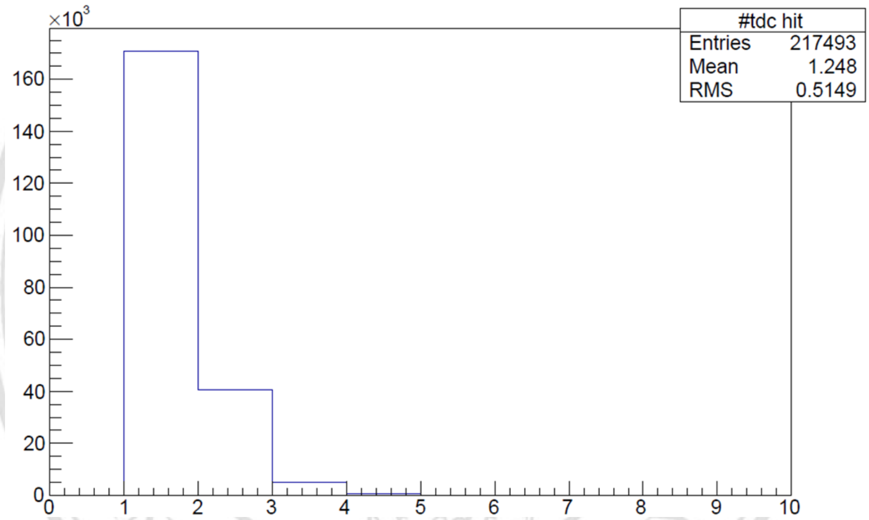

Figure 5.14: The distribution of the amount of hit times per channel

Then, the TDC time was calculated by

$$(TDC\ time) = (Recieved\ Trigger\ Time) - (The\ 1^{st}\ Hit\ Time). \tag{5.1}$$

The actual experiment of the CDC took two delay times into account for the measurement of the drift time. The incoming particle takes time to arrive the drift cell and to travel in the CDC in nanosecond time scale. For example, even if a particle move at the speed of light, the outer radius of the drift chamber is at 1130 mm, the particle needs at least approximately 4 ns to leave the detector. Moreover, the propagation time of the current pulse in the wire is not entirely neglectable. The longest wires are approximately 2400 mm, which can lead a maximum an in–wire signal delay of about 8 ns [15]. However, the inner chamber radius is only 240 mm and the longest wire is about 125 cm, thus the delay times were neglected for the test with the cosmic ray.

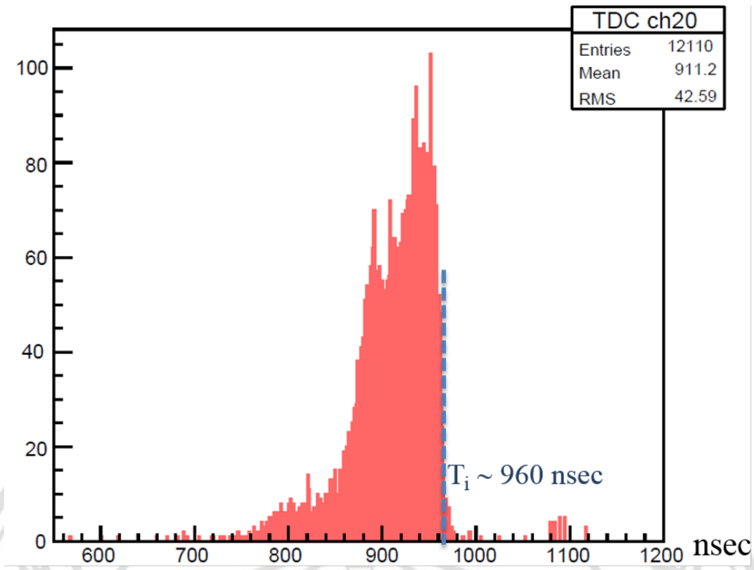

Figure 5.15: An example of TDC distribution for one channel with an approximate value of the maximum TDC time (T_i).

Figure 5.15 indicates an example of the TDC distribution for one channel with an approximate value of the maximum TDC time (T_i). The time T_i can be typically approximated by fitting the right edge of the distribution with linear equation and choosing the point that provides the maximum slope. Since the trigger time was delayed to arrive after the hit time, thus, T_i is the timing when a charged particle arrives the closest position of the wire. The time T_i is almost corresponding to the zero-distance from the wire. To calculate the drift time, the time T_i has to be subtracted from TDC time.

The drift time (ns) distribution of the inner chamber obtained from the cosmic ray test is presented in Figure 5.16 - 5.16 for each channel of the first to the eighth layer, respectively. The distributions, typically, have two edges corresponding to the drift time of the incoming particle trajectory, that close to the wire and passed the edge of the drift cell. However, the analyzed distributions still contain high frequency of noise at the right edge, such as at the channel 1, 7, 13, 19, 25, 31 and 37.

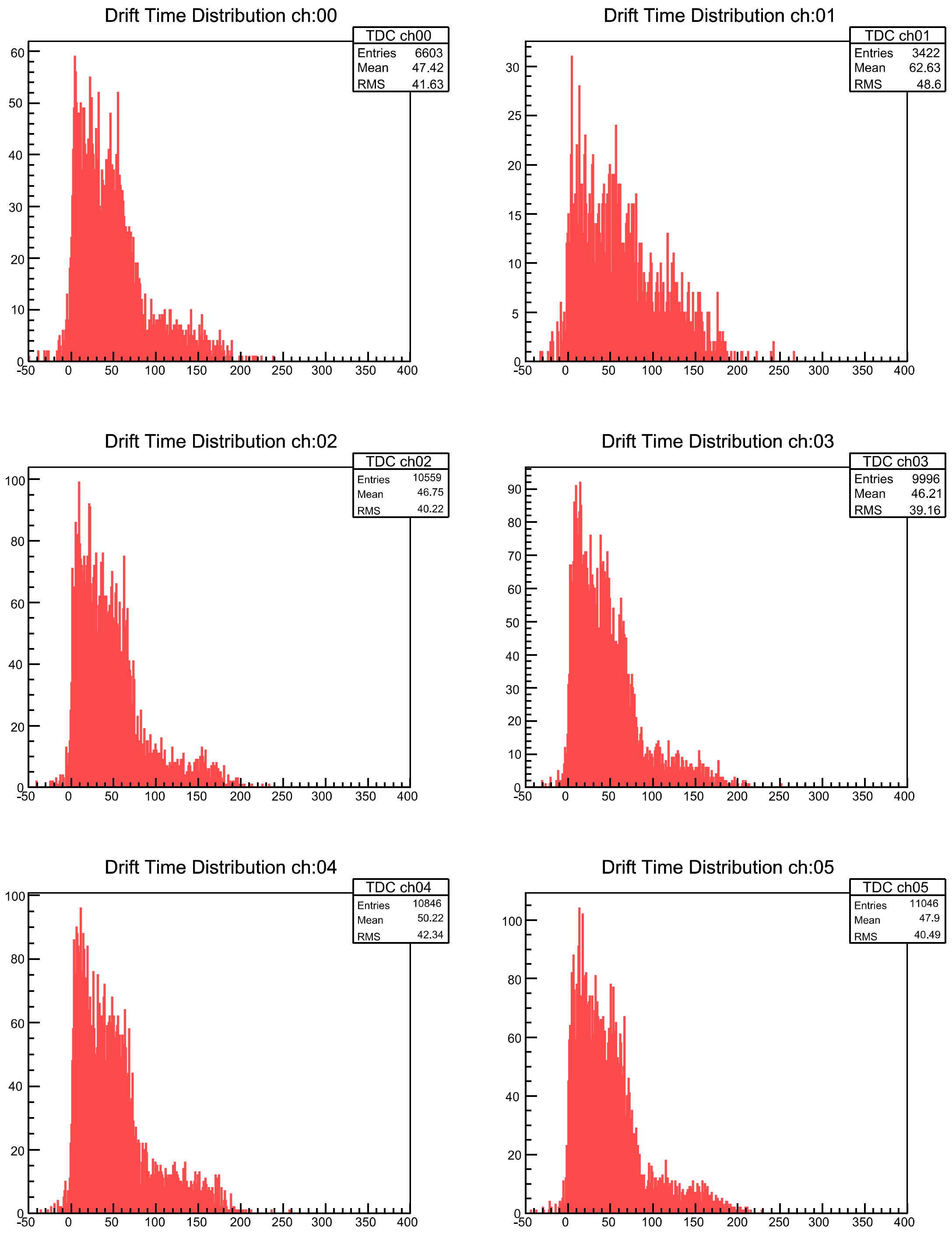

Figure 5.16: The drift time distribution (ch. 0 - 5).

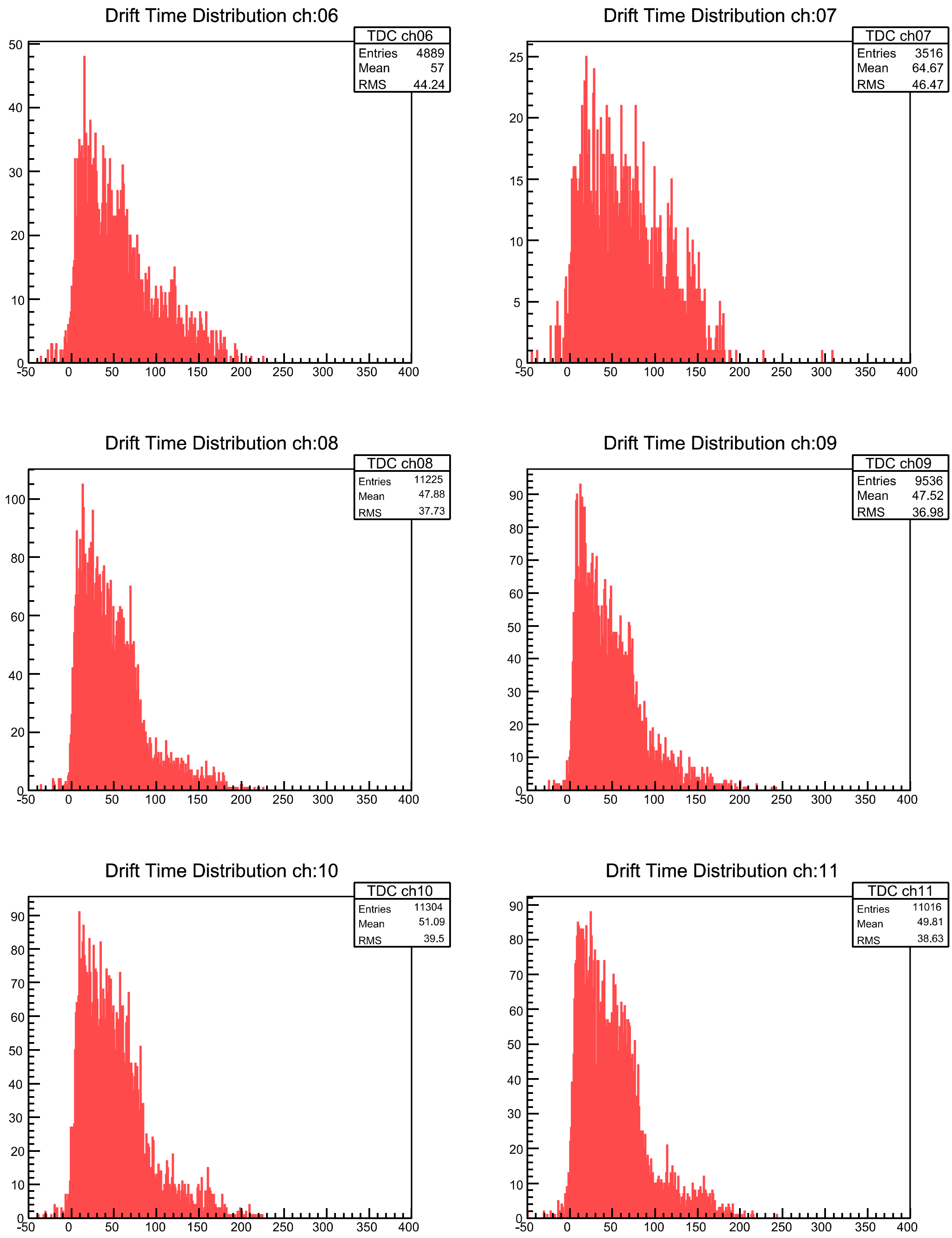

Figure 5.17: The drift time distribution (ch. 6 - 11).

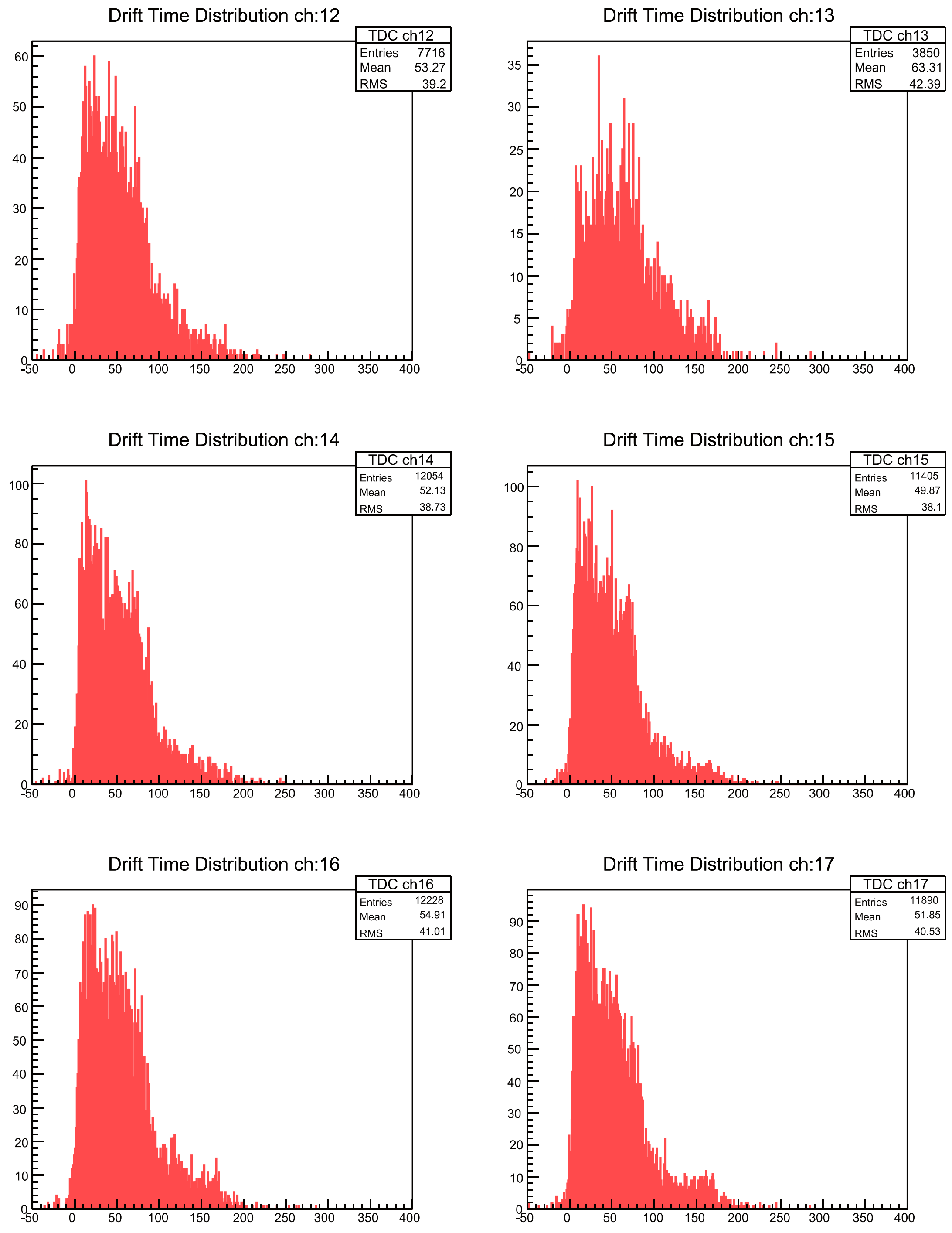

Figure 5.18: The drift time distribution (ch. 12 - 17).

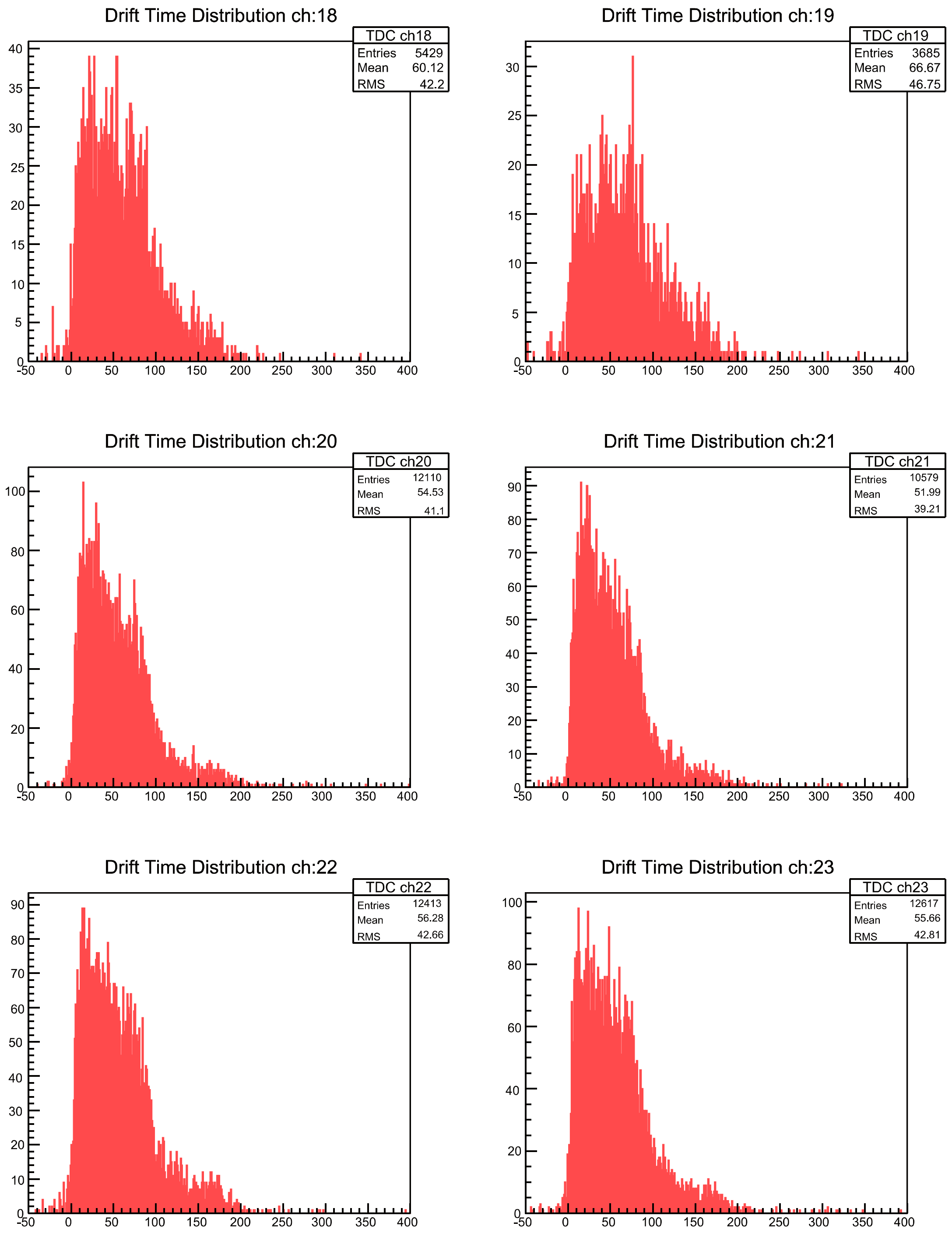

Figure 5.19: The drift time distribution (ch. 18 - 23).

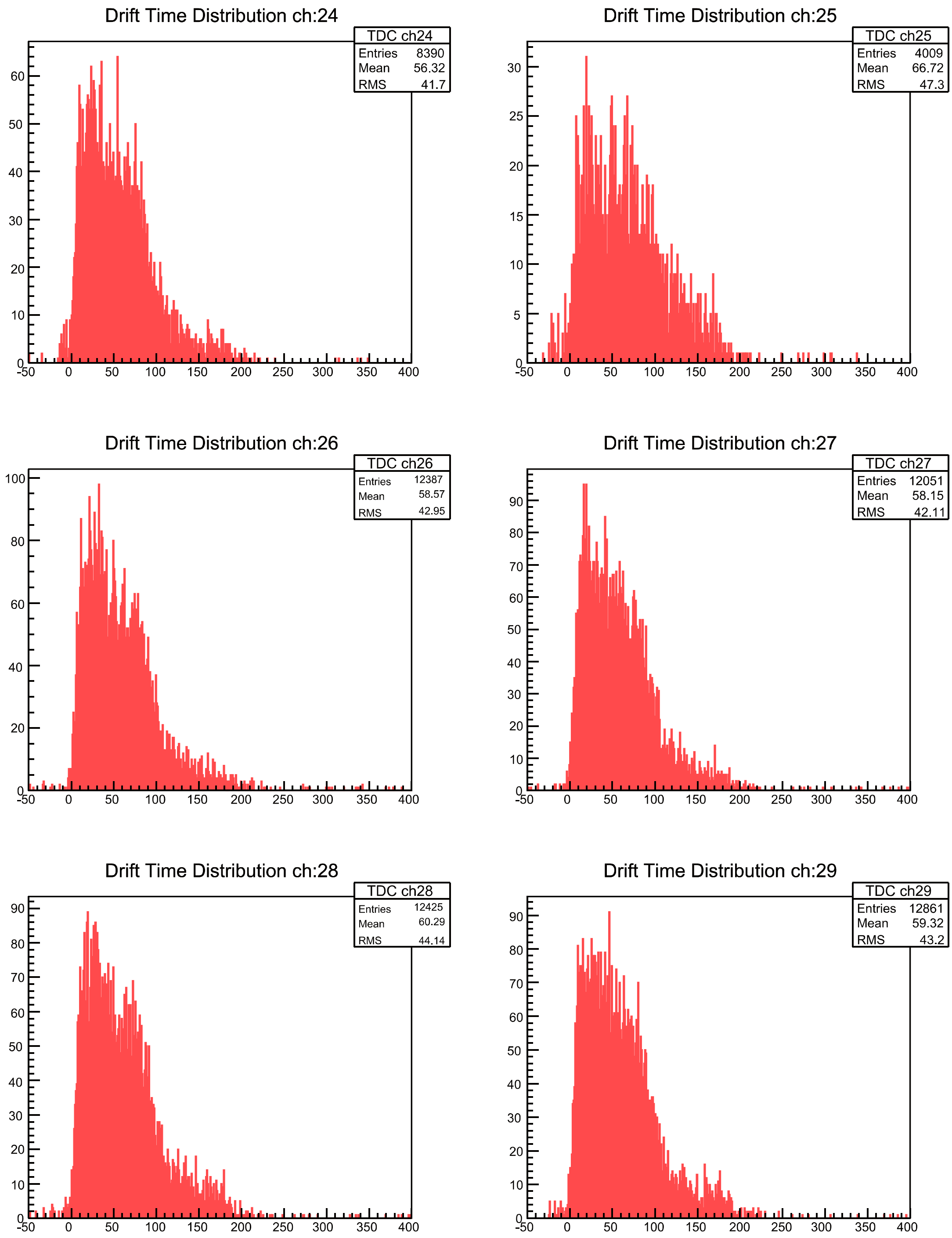

Figure 5.20: The drift time distribution (ch. 24 - 29).

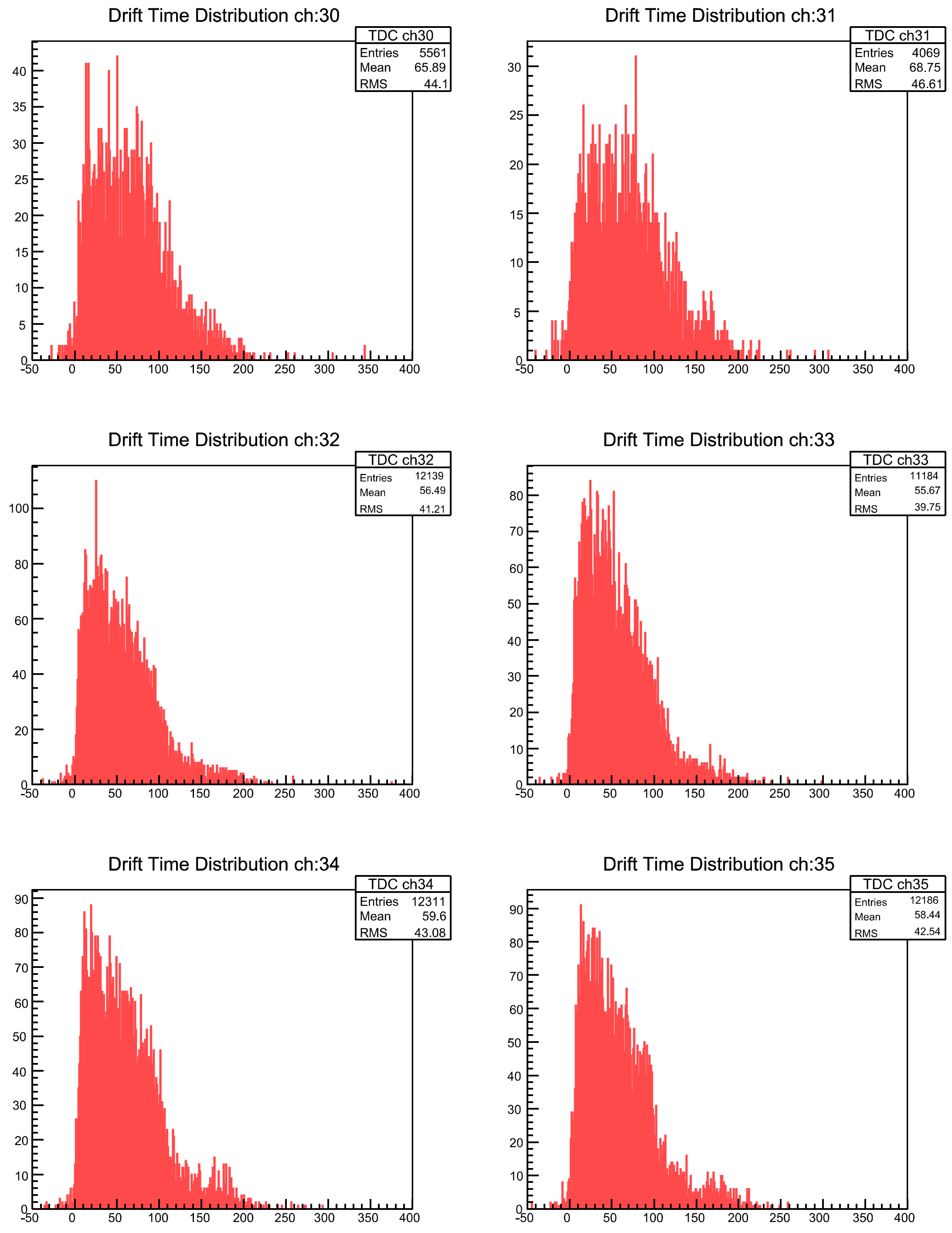

Figure 5.21: The drift time distribution (ch. 30 - 36).

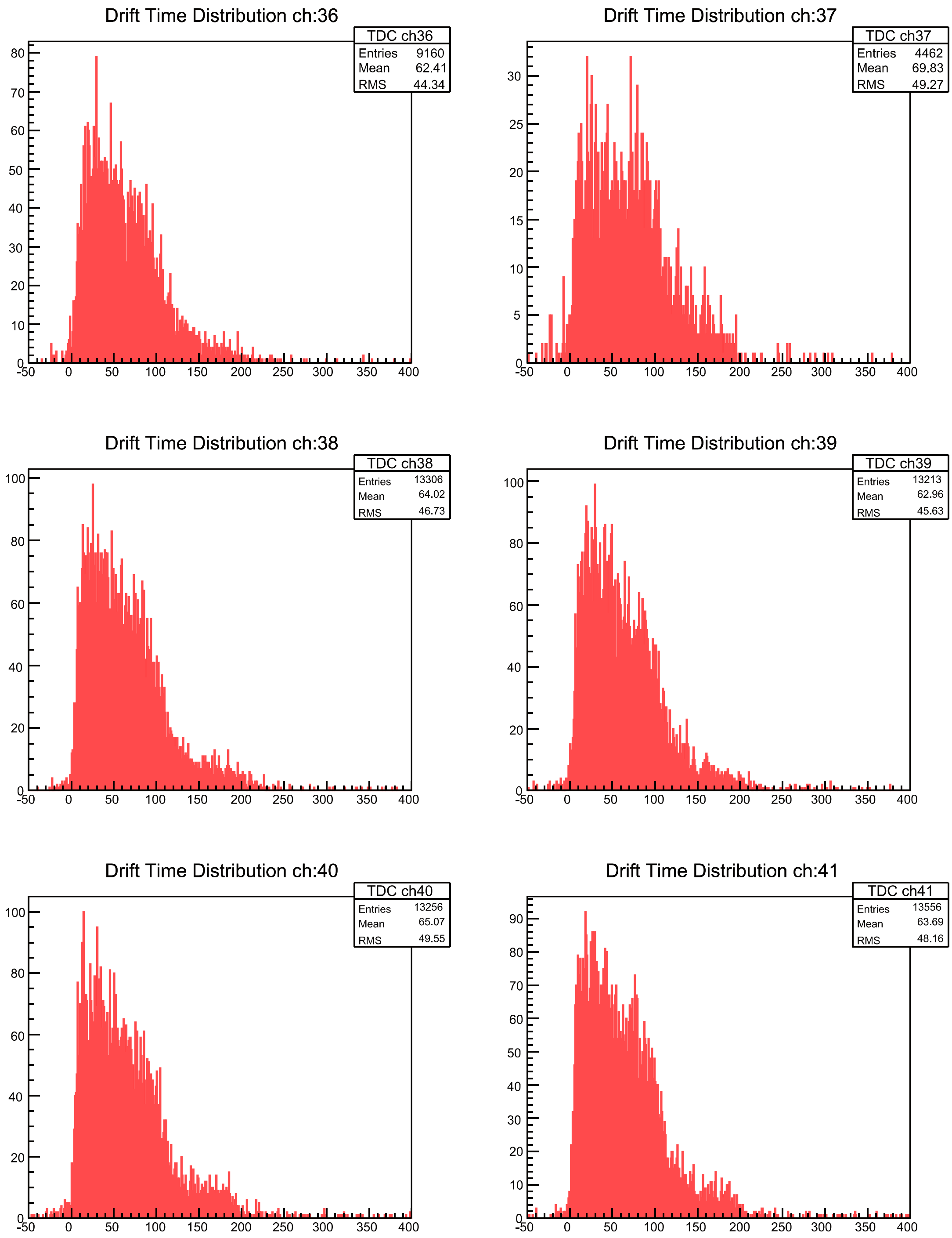

Figure 5.22: The drift time distribution (ch. 37 - 42).

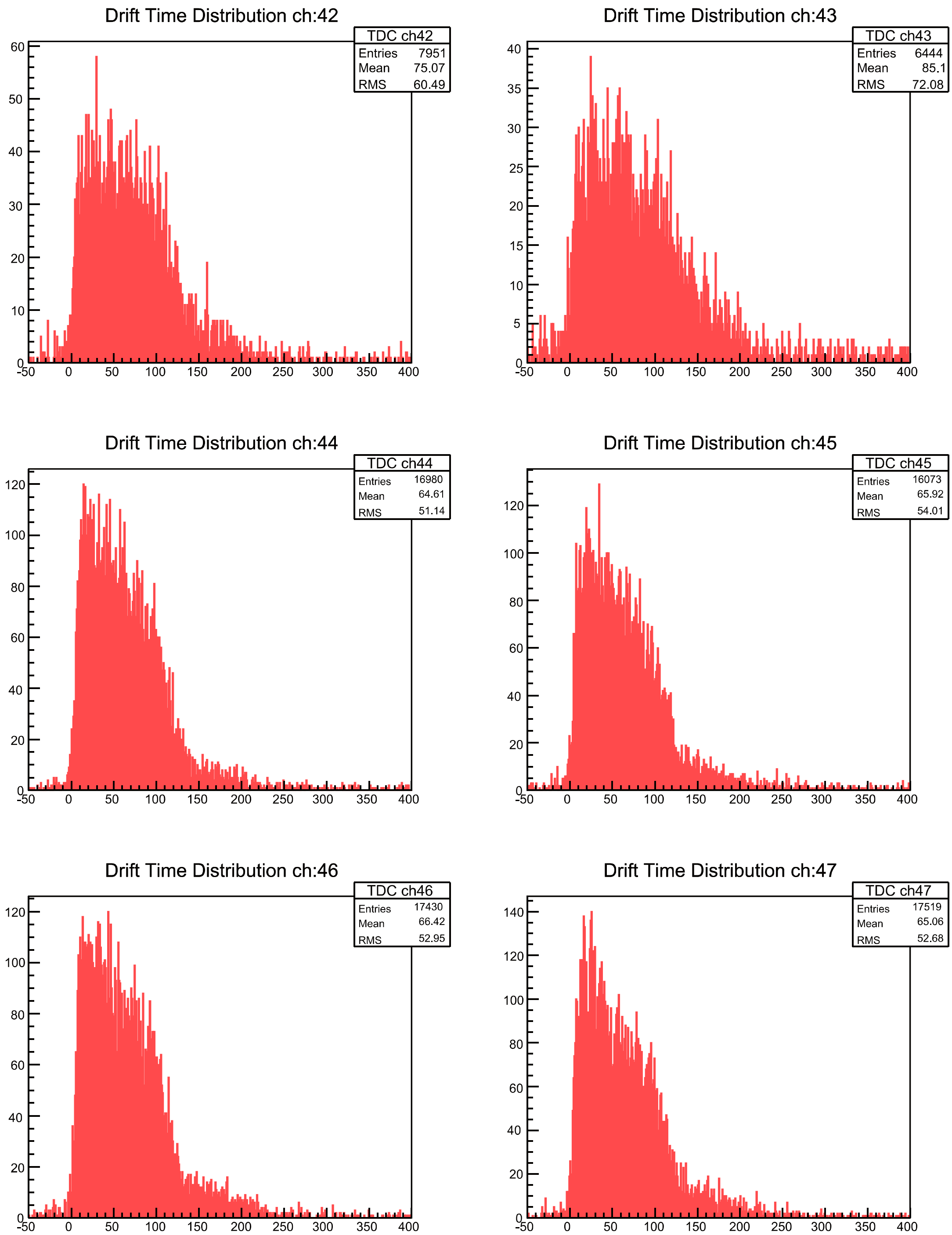

Figure 5.23: The drift time distribution (Ch. 43 - 47).

5.3 Spatial Resolution Approximation

This research focuses on the simplify method to approximate spatial resolution for the measurement with the inner chamber. There were two conditions that were used to select the data. Firstly, the events that contained two timing data consisting of trigger time and one hit time ($T1$) in each channel, called " good time ", were took into account. Figure 5.24 shows the distribution of the amount of good timing drift cell per event.Secondly, the events that contain not only the good time channel but also has only one channel in each layer were considered. Hence, the events that have eight good time channels in the distribution, which are about 11 % from all good time channels, were filtered out by the second condition to get the utilized events.

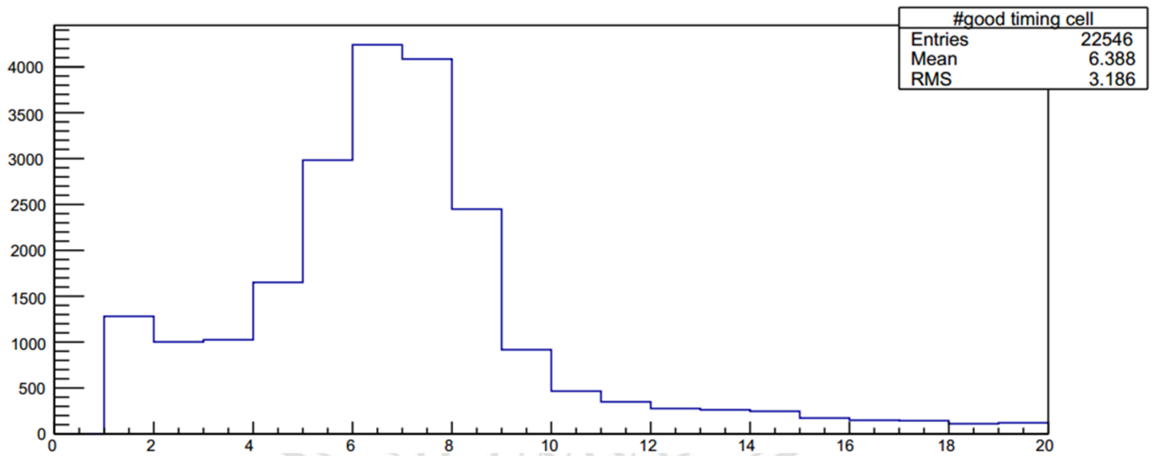

Figure 5.24: The distribution of the amount of good timing drift cell per event.

To convert the drift time to the position, that the incoming particle is generated the first ionization, the relation function between the drift time and the drift distance, X-T function, has to be calculated. In the beginning, the constant drift velocity, v_0, was assumed by approximating the minimum drift time, T_0, and maximum drift time, T_{max} from the drift time distribution. These are almost corresponding to the sense wire position and the drift cell edge or the field wire position, respectively (see figure 5.25).

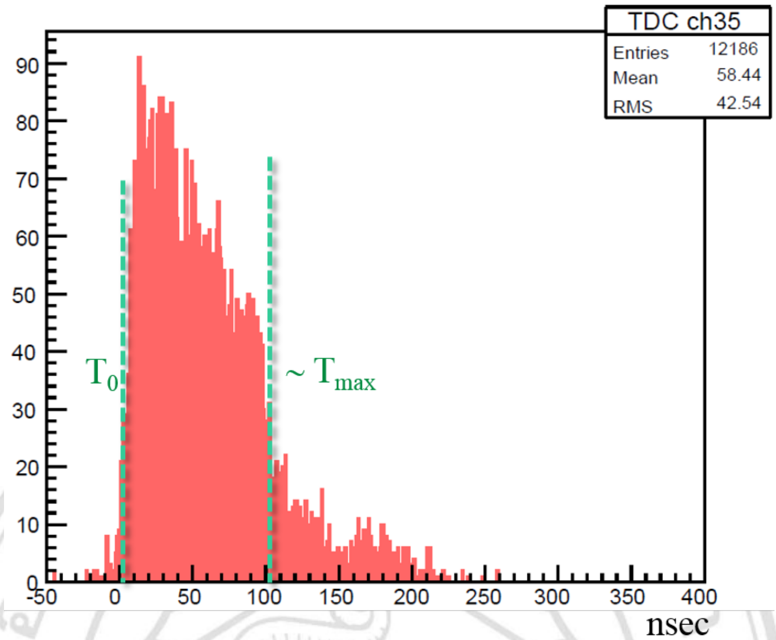

Figure 5.25: An example of drift time distribution with its, minimum drift time, T_0, and maximum drift time, T_{max}.

The distance from the sense wire position to the nearest field wire is obviously equal to the half azimuth cell size. Thus, the v_0 was calculated by

$$v_0 = \frac{half\ cell\ size(mm)}{|T_{max} - T_0|}. \tag{5.2}$$

The initial drift distance is

$$x_0 = v_0 t, \tag{5.3}$$

where x_0 is the initial drift distance(mm),and t is the drift time (ns).

In consequence, the functions of the distance to the time relation (XT relation) were obtained. The relation of the drift time, t, and the drift distance, x_0, of each channel were plotted for layer by layer. Then, the plots were fitted by the fifth order polynomial

$$x = \sum_{i=0}^{5} a_i t^i, \tag{5.4}$$

where x is the drift distance(mm), and a_i is the fitting parameter; i = 0,1,2,...,5.

The calculated drift distance, x, was used to reconstruct the particle trajectory. The position of the sense wire, which received the event signal, was used to draw a temporary trajectory. The trajectory was a straight line, hence, the linear equation was used to fit the position. When the sense wire fitted position was taken into account, which side that the particle trajectory was passed the sense wire can be checked. Thus, with the calculated x, the position that the particle collided the gas atom can be estimated. Next step, the particle trajectory was reconstructed from the linear equation fitting with the position. Then, the drift distance x was replaced by the new distance between the sense wire and the particle track.

Furthermore, the relation of the drift time and the new drift distance, x, were plotted the fifth order polynomial fitting was repeated. Therefore, the track was reconstructed again and again (self-consistent fitting). As the results, all parameters, a_i, were diverted to some constant values. The fitting parameters of each layer from the final loop of self-consistent fitting were used to estimate the spatial resolution. Figures 5.26 and 5.27 present the X-T relation plot with the final fitting line and the fitting parameters of layer 1 to 4 and 5 to 8, respectively. Figure 5.28 indicates an example of the cosmic ray reconstructed track. The red crosses represent the sense wire position and the blue circles and the radius of the calculated drift distance.

Finally, the residuals between the circumference and the track of the whole selected channel were calculated. The average spatial resolution was determined by using the Gaussian fit to each residual distribution in Figure 5.29. With 10 μm step size of the residual distribution, the spatial resolution of the inner chamber from the cosmic ray detection approximations were summarized in table 5.1.

In 2012, the spatial resolution of a test chamber with this readout electronics was estimated by the beam test . The 15 mm $\times$ 15 mm cell size test chamber was tested in the electron beam with a momentum of 1 GeV/c. The typical value of spatial resolution as small as 120 μm was obtained [14]. According to the beam test result, the cosmic ray test in this study provided the lower overall spatial resolution due to the smaller drift cell

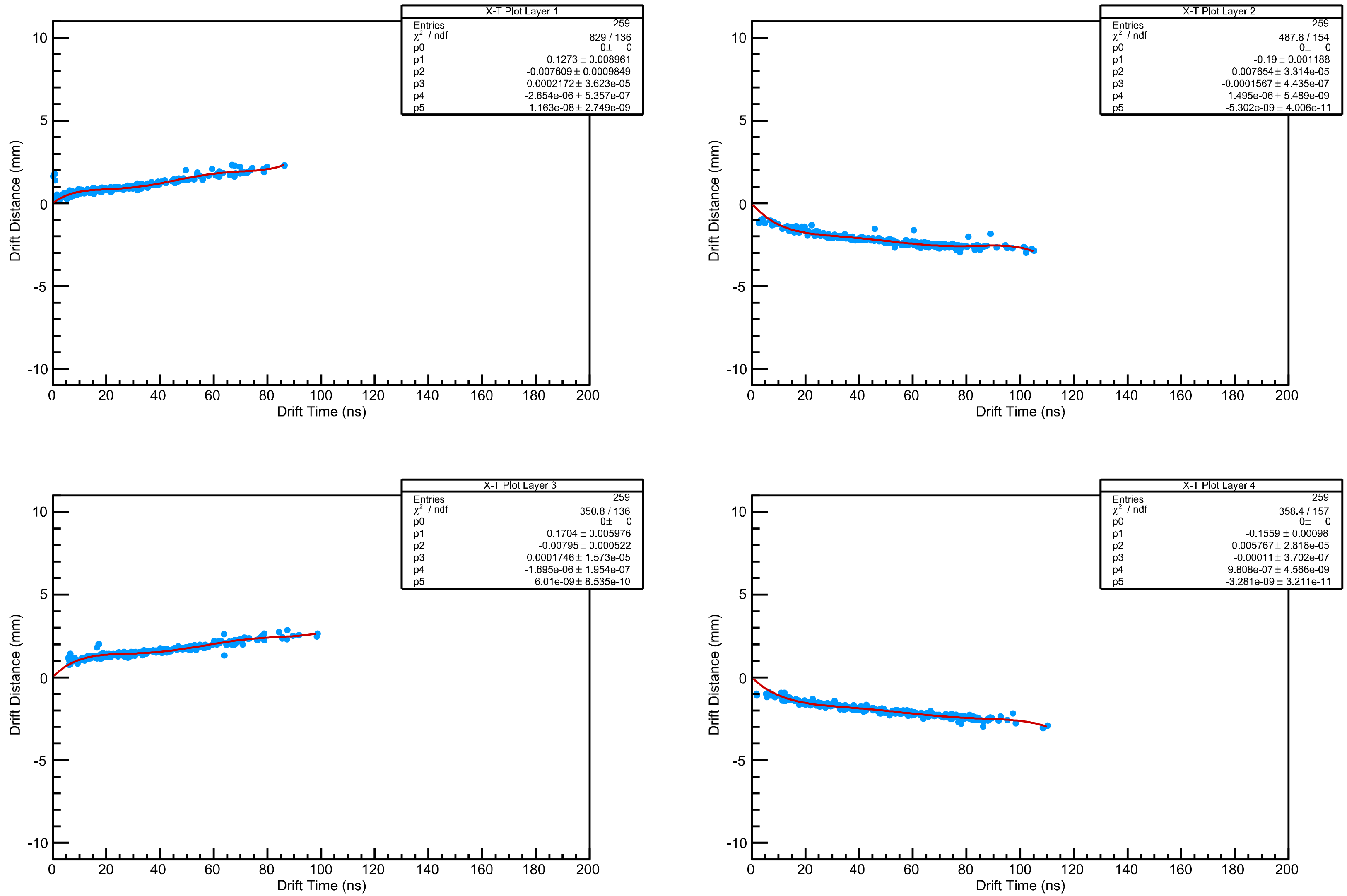

Figure 5.26: The X-T relation plot of layer 1 to 4 with the fifth order polynomial fitting.

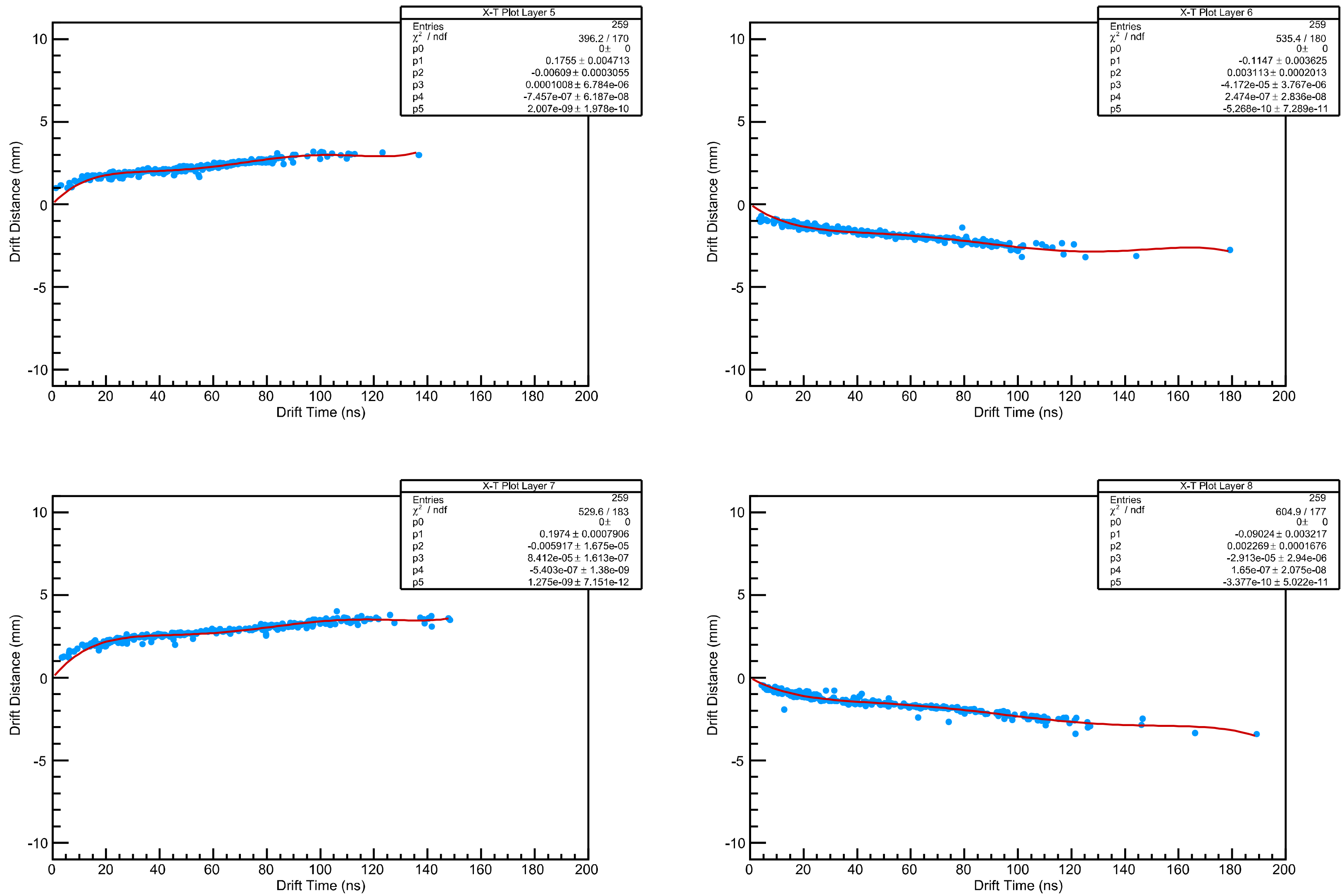

Figure 5.27: The X-T relation plot of layer 5 to 8 with the fifth order polynomial fitting.

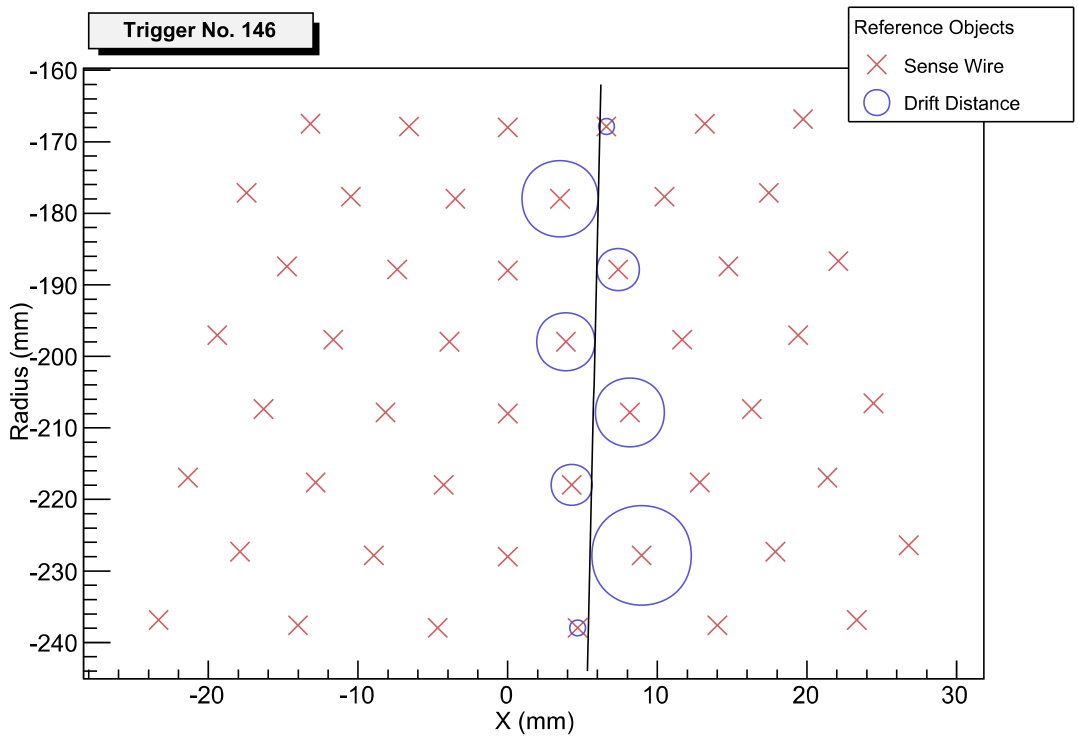

Figure 5.28: An example of the cosmic ray reconstructed track. The red crosses represent the sense wire position with the blue circles which its' radius is the calculated drift distance.

Table 5.1: The spatial resolution approximation results.

Layer	Spatial Resolution (μm)
1	86
2	81
3	77
4	76
5	90
6	104
7	108
8	98

size of the inner chamber. However, the resolution from this cosmic ray detection was approximated from too small amount of data of only 259 events following the selection conditions. Moreover, the X-T function fitting method was also different to the typical method, which is obtain by using the fitting with the fifth order polynomial and the linear function depending on the time region.

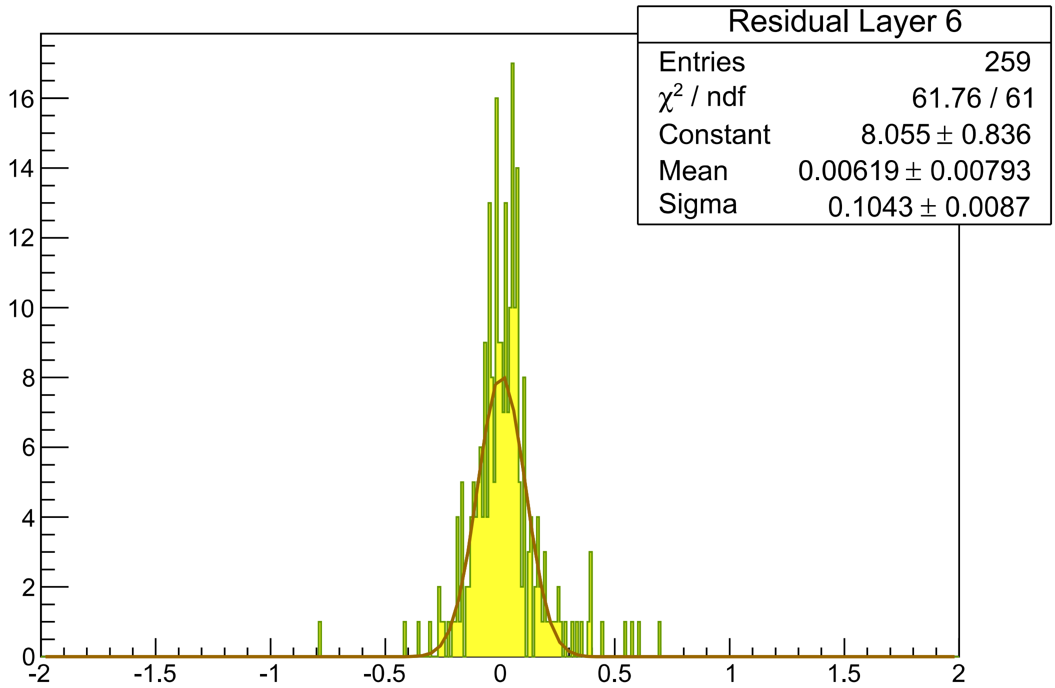

Figure 5.29: An example of the residual distribution of the layer number 6 with the Gaussian fit. The spatial resolution was approximately to be 104 μm.